

Manuscript Template

FRONT MATTER

Tropical impacts of the Southern Ocean underestimated by mean-state biases.

Authors

Title

Yue Dong,¹* Kezhou Lu,¹ Yen-Ting Hwang,² Ruei-Jia Hu,² Paulo Ceppi,³ Philipp Breul,³ Lettie A. Roach⁴, Clara Deser⁵

* To whom correspondence should be addressed. Email: ydong@atmos.ucla.edu

Affiliations

¹Department of Atmospheric and Oceanic Sciences, University of California Los Angeles, USA.

²Department of Atmospheric Sciences, National Taiwan University, Taiwan.

³Department of Physics, Imperial College London, UK.

⁴Alfred Wegener Institute, Helmholtz Centre for Polar and Marine Research, Germany.

⁵Climate and Global Dynamics Division, National Center for Atmospheric Research,

USA.

Abstract

The observed sea-surface temperature (SST) trends over recent decades feature cooling in the tropical eastern Pacific and the Southern Ocean (SO). Growing evidence suggests that tropical cooling trends may partly stem from remote impacts of the SO. Using a hierarchy of multi-model simulations, we demonstrate that these teleconnections are robustly modulated by the mean-state inter-tropical convergence zone (ITCZ): models with a more realistic ITCZ structure simulate a stronger tropical SST response to SO forcing via stronger surface winds in the tropical eastern Pacific. When realistic Antarctic meltwater forcing is accounted for, correcting the model's tropical mean-state bias yields a stronger tropical cooling response to meltwater-driven SO cooling, improving the agreement between simulated and observed SST trends. Our results suggest that the SO's contribution to tropical warming patterns is systematically underestimated due to model mean-state biases. Improving representations of SO teleconnections is critical for accurately assessing historical and future warming patterns.

Teaser

The Southern Ocean's contribution to the observed tropical La Niña-like warming pattern has been systematically underestimated due to model mean-state biases

MAIN TEXT

Introduction

Observations over recent decades have exhibited a distinctive sea-surface temperature (SST) trend pattern, characterized by broad cooling in the tropical eastern Pacific and the Southern Ocean (SO) (1, 2). This observed SST trend pattern has been linked to a wide range of changes in climate and extreme events across regional to global scales (3-6).

However, reproducing this pattern remains a challenge for Global Climate Models (GCMs) participated in the Climate Model Intercomparison Project Phase 5 (CMIP5) and Phase 6 (CMIP6) (1, 2, 7), calling into question the credibility of GCM-based future climate projections.

A diverse pool of mechanisms has been put forward to explain the observed tropical SST trend pattern and model-observational discrepancies (2, 8); however, consensus has yet to be reached on their relative importance. Tropical eastern Pacific cooling may arise from the transient oceanic response to greenhouse gas (GHG) forcing via the ocean thermostat mechanism (9, 10), which indicates a possible persistence of the recent La Niña-like warming pattern into the near future under continued GHG forcing. On the other hand, contributions of anthropogenic aerosol emissions (11) and natural variability in the Pacific (12, 13) may point to a possible shift toward an opposite El Niño-like warming pattern in the future. Unraveling the causes of the recent historical SST pattern is therefore critical for accurately predicting its future evolution.

Among the proposed mechanisms, remote impacts from the SO have received increasing attention. Like the tropical eastern Pacific, the SO has experienced significant SST cooling over recent decades, particularly in the eastern Pacific sector (1, 14). Various modeling evidence has revealed that SO cooling can drive a tropical La Niña-like SST response through atmospheric and oceanic teleconnections (14-18), suggesting a potential extratropical origin of the observed tropical cooling trends. Indeed, recent studies demonstrated that a La Niña-like tropical SST pattern can arise from Antarctic ice-sheet meltwater input (19) and Antarctic ozone depletion (20, 21), both of which are leading hypotheses for the observed SO cooling (22-25). Furthermore, directly nudging the observed SO SST anomalies in a fully-coupled GCM improved the agreement between simulated and observed tropical SST patterns (18), highlighting the SO's role as a pacemaker of tropical and global climate change (26).

However, several gaps remain in our understanding of the SO's contribution to the recent and near-future tropical warming patterns. First, although a La Niña-like tropical SST response to SO cooling is consistently simulated, models often use idealized SO forcings that are unrealistically strong (27), or simulate a tropical SST response that is weaker than observed (19). Second, existing modeling work exhibits varying degrees of tropical SST response (17, 18, 28), reflecting a wide spread in the strength of SO teleconnections. Furthermore, while the Southern Hemisphere (SH) subtropical eastern Pacific SST response is relatively robust, large uncertainty exists in the *equatorial* SST response (19, 29), which governs remote impacts on the northern hemisphere (NH) hydroclimate (30, 31) and global warming rate (32). Ultimately, despite progress from numerical model experiments, we are left with the question: to what extent has the SO contributed to the recent tropical SST trends and global climate change observed in nature?

In this study, we aim to better constrain the SO teleconnection strength by examining the key physical processes that modulate the SO teleconnections in individual GCMs and their inter-model spread. We focus specifically on two factors: subtropical cloud feedback and the tropical mean-state climate. Subtropical cloud feedback has been identified as a major contributor to the inter-model spread in SO teleconnection strength (17). The tropical mean state—particularly precipitation and surface winds—likely also plays a critical role in shaping the tropical SST response to SO forcings, yet its influence remains poorly understood. Like cloud feedbacks, tropical mean-state biases are prevalent in GCMs, most

notably associated with the Intertropical Convergence Zone (ITCZ) known as the "double-ITCZ" problem (Fig. S1) (33, 34). While such mean-state biases may directly affect the local SST response to CO₂ forcing (9, 35), here we focus on the tropical SST response to remote SO forcings and ask: do tropical mean-state biases affect the simulated strength of SO-tropical Pacific teleconnections? If so, what are the implications for understanding the observed tropical warming pattern?

To address these questions, we leverage multiple lines of evidence, including a suite of idealized simulations with the Community Earth System Model version 1 (CESM1, a CMIP5-class GCM), two multi-model intercomparison projects that uniquely incorporated SO thermal and freshwater forcings, and ensembles of transient historical simulations with realistic SO corrections using the NASA Goddard Institute for Space Studies version E2.1 climate model (GISS-E2-1-G, a CMIP6-class GCM). By comparing model results with observations, we provide new constraints on the remote tropical impact of SO SST changes.

Results

Sensitivity of the SO-tropical Pacific teleconnection strength

We begin by presenting results from idealized simulations with the slab-ocean configuration of CESM1 (Methods). To isolate the impacts of subtropical cloud feedbacks and the tropical mean state, we conduct three sets of control and SO-cooling simulations. The three control runs feature distinct mean-state climates, namely: (1) a "base" mean state, derived from a long control simulation of the fully-coupled CESM1, which carries all intrinsic model biases; (2) a "flux-adjusted" mean state, in which we modify climatological surface heat fluxes ("qflux") to better align the simulated SST and precipitation patterns with observations; (3) a "cloud-adjusted" mean state, in which we modify the model's radiation code to increase low-cloud-SST sensitivity over the subtropical stratocumulus deck to better match satellite observations. For each mean state, we perform a corresponding SO cooling experiment by imposing a constant qflux anomaly in the SO to induce local SST cooling (Methods).

First, we show the mean-state differences across the three control runs. Focusing on the tropical zonal-mean precipitation (Fig. 1C), the "base" control run exhibits a typical "double-ITCZ" bias, similar to other CMIP6 models. The "cloud-adjusted" control run produces a nearly identical precipitation pattern, retaining the same double-ITCZ bias. In contrast, the "flux-adjusted" control run substantially improves the ITCZ representation, producing a more asymmetric precipitation pattern that closely matches observations (Fig. 1C and Fig. S2). This is because the "flux adjustment" effectively changes the mean-state SST distribution (Fig. S3A) and therefore precipitation patterns (Fig. S3B). By contrast, the "cloud adjustment" is designed to increase the sensitivity of low cloud amount to instantaneous SST anomalies relative to the mean state. Although this significantly increases the SST variance in the tropical eastern Pacific (36), it does not affect the SST mean state averaged over a long period (Fig. S3D; see also ref (36) for similar results using fully-coupled CESM1). Meanwhile, the shortwave (SW) cloud-SST feedback (λ_{cldsw}) over the SH subtropical eastern Pacific region substantially strengthens in the "cloud-adjusted" control run (Fig. S3F), while remaining largely unchanged in the "fluxadjusted" control run (Fig. S3C). Overall, the "flux-adjustment" reduces the double-ITCZ

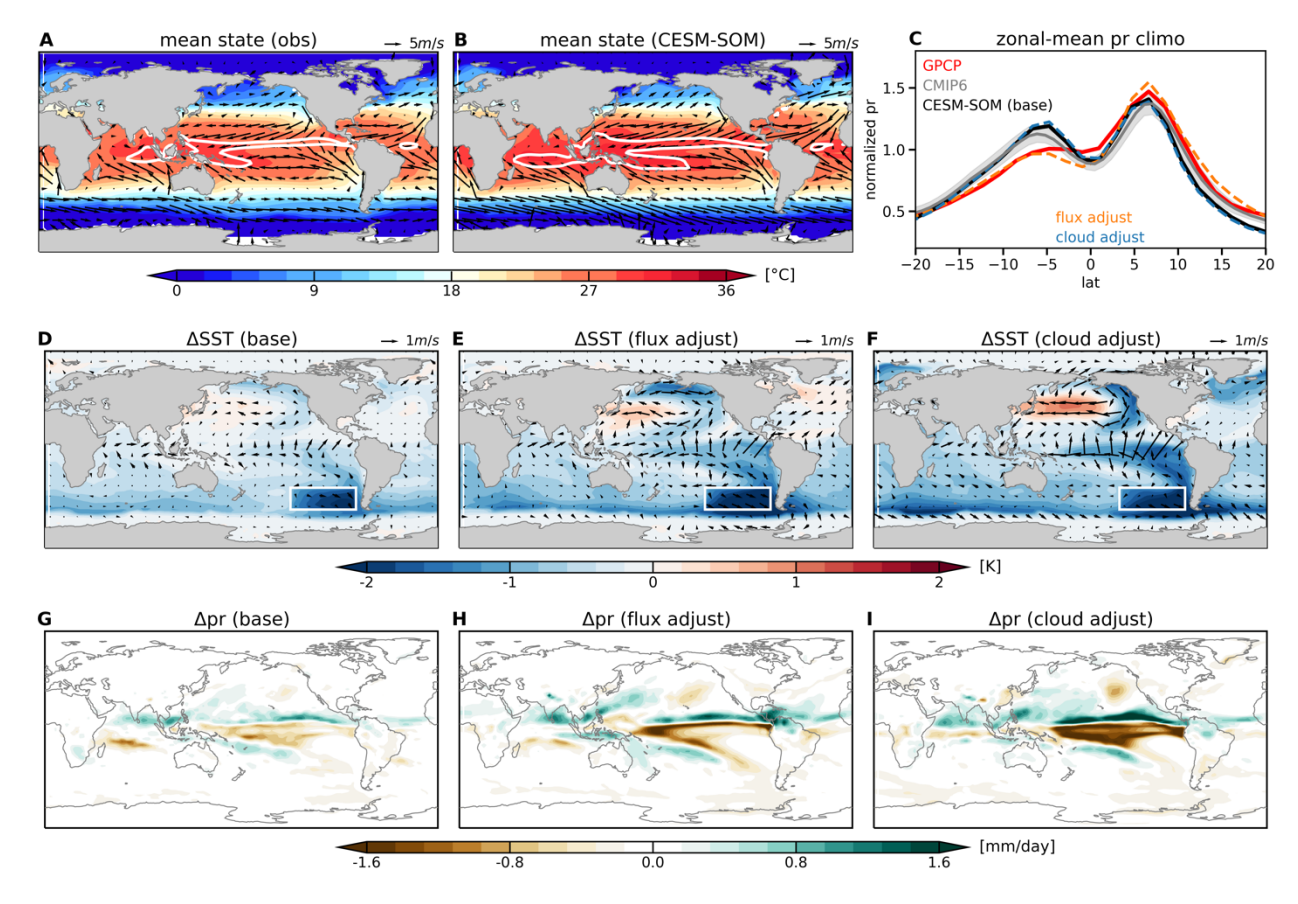


Figure 1: Mean-state climate and simulated response to Southern Ocean aflux perturbation in CESM1. (A, B) Annual-mean climatology of SST (shading), surface winds (arrows), and precipitation (white contour denotes 6.5 mm/day level) in (A) observations and (B) CESM1 "base" control run. (C) Zonal-mean annual-mean precipitation normalized by the tropical mean from GPCP observations (red), CMIP6 multi-model mean (grey), CESM1 "base" control run (black), "flux-adjusted" control run (orange) and "cloud adjusted" control run (blue). The grey shading denotes one standard deviation across CMIP6 models. (D-F) Simulated annual-mean SST (shading) and surface wind (arrows) response to the imposed aflux perturbation in the "base", "flux-adjusted", "cloud-adjusted" simulations, respectively. White box illustrates where the anomalous aflux forcing is imposed (Methods). (H-I) Simulated annual-mean precipitation response.

We next examine the quasi-equilibrium tropical response to the imposed SO qflux forcing (over the white box in Fig. 1D–F). With the "base" mean state, the imposed SO cooling produces a remote tropical response (Fig. 1D), including a La Niña-like cooling, strengthened SH trade winds, and a northward displacement of the ITCZ. This response pattern resembles the previously identified SO teleconnection response (14, 15, 27), driven by a series of coupled processes: SO SST anomalies are first advected into the tropics by mean winds in the southeast Pacific, initiating an anomalous zonal SST gradient; this SST gradient is further amplified by subtropical cloud feedback and the wind-evaporation-SST (WES) feedback in the tropical eastern Pacific (14, 17). These tropical responses strengthen further in the flux- and cloud-adjusted mean states. Both adjustments produce stronger tropical eastern Pacific SST cooling (Fig. 1E, F), enhanced tropical zonal SST gradients (Fig. S4A), and more pronounced precipitation anomalies (Fig. 1H, I, Fig. S4B). Notably, with the mean-state adjustments, the remote SST and precipitation responses extend further into NH midlatitudes (Fig. 1) exerting more

widespread global impacts. The results suggest that both subtropical cloud-SST feedback and the mean ITCZ structure are critical for the remote response to SO cooling, and that biases in either may lead to underestimation of the teleconnection. While our simulations correct these two biases separately by design, we next ask: do they influence the tropical response through independent mechanisms?

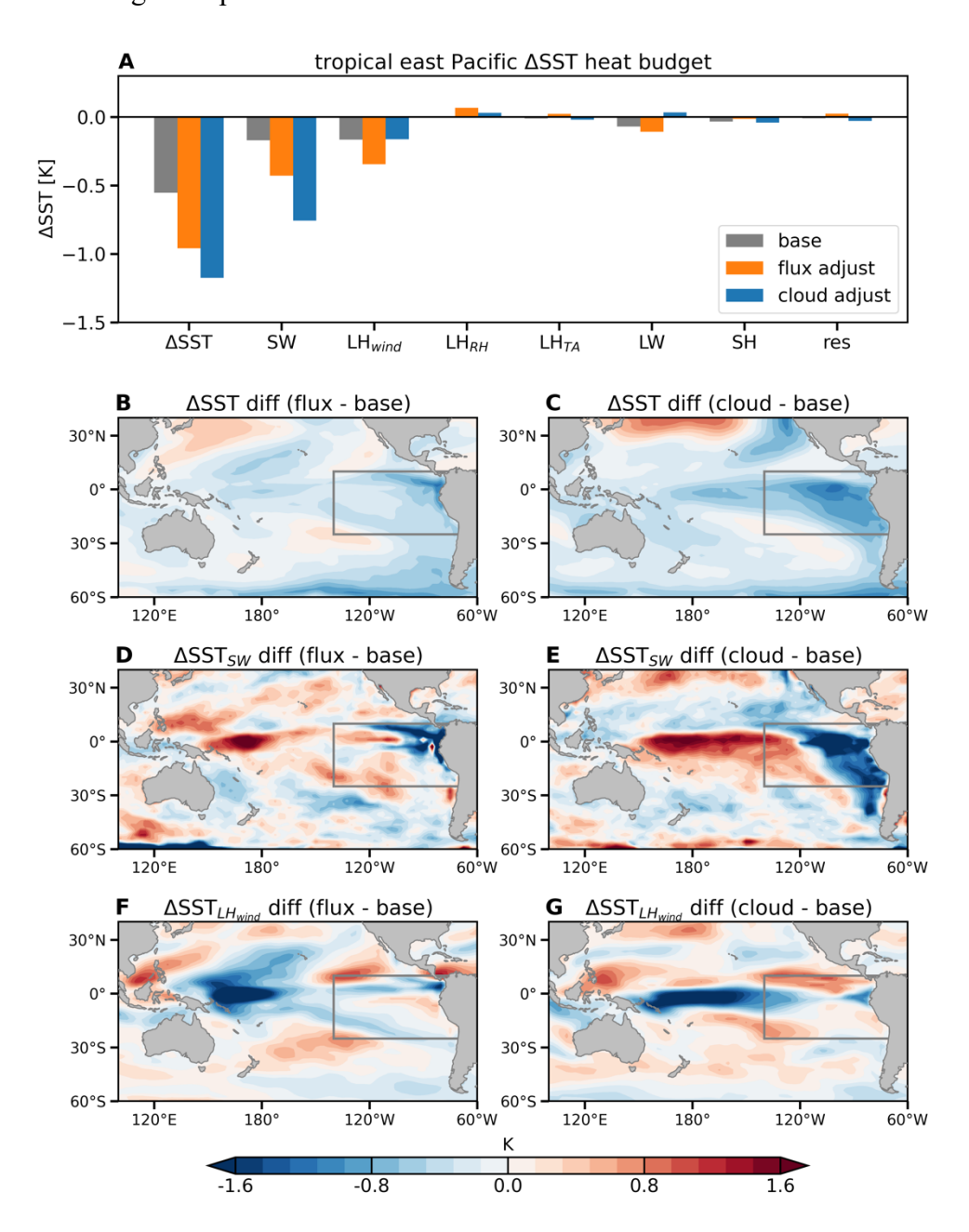


Figure 2: Surface energy budget analysis for the simulated tropical SST response in CESM1 simulations. (A) Contributions of individual energy flux terms to the SST response averaged over the tropical eastern Pacific (the grey box illustrated in panels B–G). From left to right are actual simulated SST response (Δ SST), contributions from shortwave flux (SW), latent heat flux due to wind speed changes (LH_{wind}), latent heat flux due to relative humidity changes (LH_{RH}), latent heat flux due to stability (LH_{TA}), longwave flux (LW), sensible heat flux (SH), residual (res). (SH-G) Difference in the actual SST response (SH, SW-induced SST response (SH, SW-induced SST response (SH), and the SW-induced SST response (SH) between "flux-adjusted" and "base" runs (left), and between "cloud-adjusted" and "base" runs (right).

To understand the mechanisms, we perform a mixed-layer heat budget analysis of the tropical SST cooling response in all three simulations (Methods). Focusing on the broad

Science Advances Manuscript Template Page 5 of 19

tropical eastern Pacific region (box in Fig. 2B–G), we find that the SW radiative effect and the latent heat effect due to changes in wind speed (LH_{wind}) consistently dominate the SST response, confirming the leading roles of low cloud feedback and the WES feedback (17, 18, 37). However, their relative roles and spatial patterns differ across mean states. In the "cloud-adjusted" run, the tropical eastern Pacific SST cooling is predominantly driven by SW flux (Fig. 2A), which accounts for most of the additional cooling relative to the "base" simulation (Fig. 2E). In contrast, the "flux-adjustment" produces stronger tropical cooling primarily through an enhanced WES feedback (Fig. 2A) over the subtropical trade wind regions (Fig. 2F), with the cloud feedback making limited contribution confined to areas off the coast of south America (Fig. 2D). The enhanced WES feedback is associated with the improved ITCZ mean state (Fig. S3A), characterized by stronger trade winds in the SH subtropical eastern Pacific and cross-equatorial southerlies converging into the band of deep convection north of the equator. These intensified mean-state winds enable stronger advection of SO SST anomalies into the tropical central Pacific and equatorial eastern Pacific, and also enhance the WES feedback further amplifying the cooling.

Overall, the idealized CESM1 simulations suggest that, in addition to the subtropical cloud feedback, the ITCZ representation is also critical to the strength of SO-tropical Pacific teleconnections. Importantly, the effect of an improved ITCZ is independent of improved cloud feedback in our model, implying an additional and previously underappreciated role for mean-state ITCZ modulation of SO teleconnections.

Inter-model spread in tropical response to SO SST forcing

Building on the CESM1 slab-ocean simulations, next we revisit the inter-model spread in the tropical response to SO cooling provided by the Extratropical-Tropical Model Inter-comparison Project (ETIN-MIP) (27). In the ETIN-MIP fully-coupled simulations used here, solar flux is reduced between 65°S and 45°S to force the SH extratropical surface temperature to cool, which subsequently drives a La Niña-like response in the tropical Pacific (16, 17, 27). Although this tropical response is robust in the multi-model mean (Fig. 3D), its pattern and magnitude vary widely across individual models (Fig. S5). As shown in ref. (17), the inter-model diversity in the tropical responses can be attributed to differences in subtropical cloud feedback off the west coast of South America (CF_{wSA})—models with a larger CF_{wSA} tend to produce a greater SST cooling response in the subtropical eastern Pacific.

Is the inter-model spread in the tropical SST response across ETIN-MIP also connected to models' ITCZ biases, as indicated by our CESM1 simulations? A first look at the precipitation mean state in ETIN-MIP's control simulations reveals diverse ITCZ structures across the models (Fig. 3A), but nearly all exhibit a consistent double-ITCZ bias. To quantify the bias, we define a precipitation asymmetry metric (pr^*) as the difference between NH and SH zonal-mean precipitation maxima, normalized by the tropical mean precipitation (Methods). Changing the precipitation averages to the Pacific yields similar results. Most models simulate a pr^* smaller than the observed (Fig. 3B), reflecting the double-ITCZ bias. We further regress the tropical eastern Pacific SST response to SH cooling (white box in Fig. 3D) onto each model's mean-state pr^* across all seven models. A significant correlation is obtained (Fig. 3B), with pr^* explaining ~75% of the inter-model variance in the tropical eastern Pacific SST response. Models with a larger pr^* tend to simulate a stronger tropical eastern Pacific SST cooling response to SO

forcing. A global regression of SST response onto pr^* also confirms its broad influence on the tropical SST pattern (Fig. 3F).

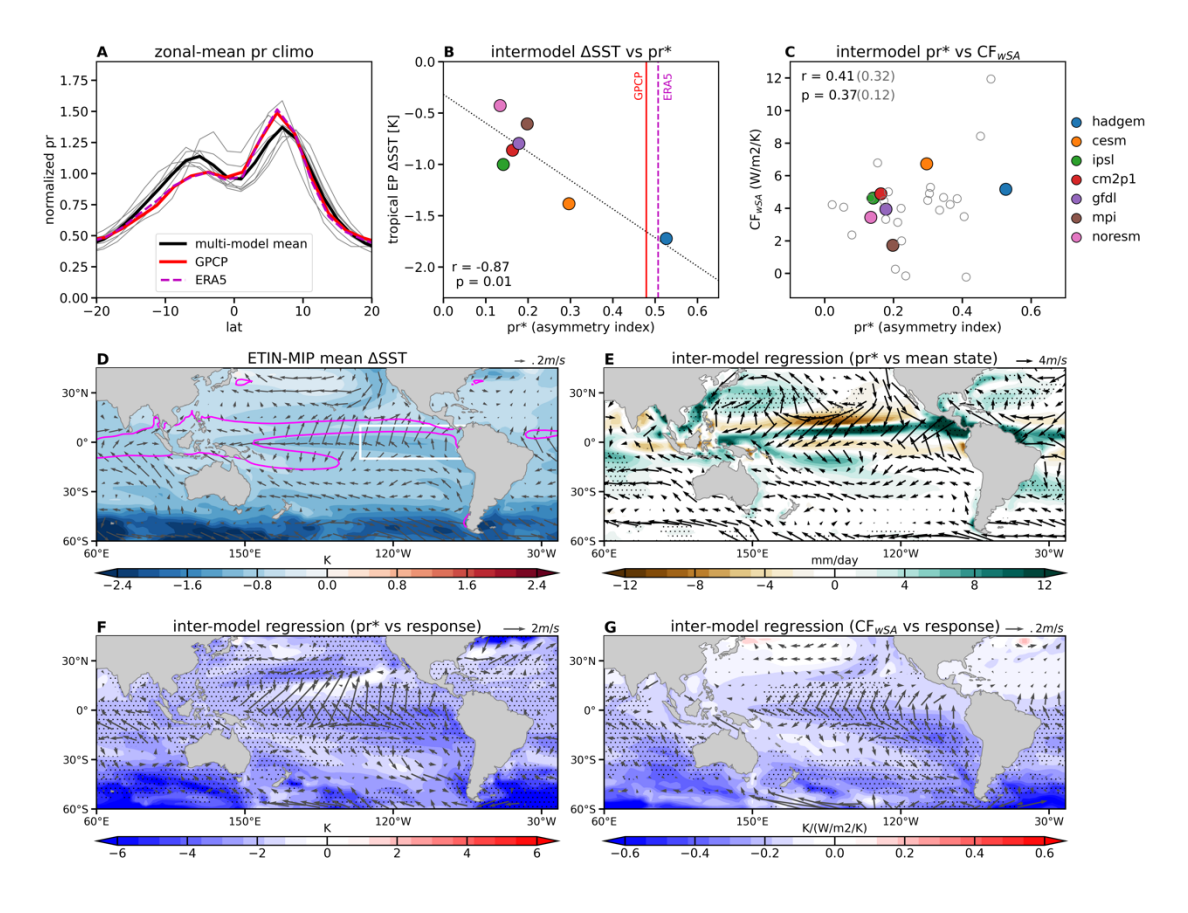


Figure 3: Mean-state climate and response to SO forcing in ETIN-MIP experiments. (A) Annual-mean zonal-mean precipitation normalized by the tropical mean from observations and ETIN-MIP models. Solid red line denotes GPCP observations, dashed magenta line denotes ERA5; thick black line denotes the average of seven ETIN-MIP models, and thin grey lines denote individual models. (B) Inter-model correlation between tropical eastern Pacific SST response (the white box illustrated in panel D) and mean-state pr*. (C) Inter-model correlation between mean-state pr* and subtropical cloud-SST feedback (CF_{wSA}) for ETIN-MIP models (colored scatters) and 24 CMIP6 models (grey unfilled scatters). Correlation coefficient (r) and p-values for ETIN-MIP and CMIP6 inter-model correlations are shown in black and grey text, respectively. (D) ETIN-MIP multi-model mean SST and surface wind response to SH extratropical forcing. Magenta contour denotes the 6 mm/day level of the annual-mean climatological precipitation. (E) Inter-model regression between mean-state precipitation and surface winds onto pr*. (F) Inter-model regression between local SST and surface wind response onto Pr*. (G) Inter-model regression between local SST and surface wind response onto CF_{wSA}. Stippling denotes where the inter-model regression is statistically significant at the 95% confidence level.

How does the mean-state ITCZ influence the tropical SST response to SO forcing? We show in Fig. 3E that models with a larger pr^* tend to simulate a mean-state climate with more (less) precipitation in the north (south) of the equator, as well as stronger surface southeasterly winds in the subtropical southeastern Pacific and more pronounced southerlies along the equator. As demonstrated in the CESM1 "flux-adjusted" simulations, stronger mean winds promote the advection of SST anomalies from the SO to the tropical Pacific and enhance the WES feedback, thereby amplifying the SST cooling response in the trade wind regions (Fig. 3F). Although the CESM1 simulations are conducted in a slab-ocean configuration and the ETIN-MIP results are obtained from fully-coupled GCMs, the resemblance between the two datasets strongly supports the mechanism by which the ITCZ modulates SO teleconnections.

That said, it is unclear whether the inter-model spread in the ITCZ biases (pr^*) is correlated with—if not caused by—the spread in subtropical cloud feedback (CF_{wSA}). It has been proposed that biases in subtropical cloud feedback may contribute to the double ITCZ biases by locally influencing eastern Pacific SSTs (38). Here we regress pr^* onto CF_{wSA} across the seven ETIN-MIP models, and find the correlation is overall positive but insignificant (Fig. 3C). This weak positive correlation is also evident in the piControl simulations from the broader CMIP6 models (grey scatters in Fig. 3C), with a correlation coefficient of only 0.32. These results suggest that although models with a more realistic ITCZ structure generally tend to also have a stronger subtropical cloud feedback, the spread in the ITCZ and the spread in cloud feedback are more likely associated with other independent factors. Furthermore, by regressing the SST response to SH cooling at each grid box onto pr^* (Fig. 3F) and CF_{wSA} (Fig. 3G), we find notable differences in their spatial patterns: stronger cloud feedback (larger CF_{wSA}) is associated with stronger cooling mostly in the subtropics, whereas better ITCZ (greater pr^*) is linked to more widespread cooling that can extend into the equatorial eastern Pacific. This is because models with a more realistic ITCZ also simulate stronger cross-equatorial meridional winds (Fig. 3E), which enables the advection of SST anomalies into the deep tropics, consistent with the "flux-adjusted" CESM1 simulation (cf. Fig. 3B and 3C).

In summary, the inter-model spread in the tropical SST response across ETIN-MIP models is associated with differences in the mean-state ITCZ, and this effect is largely independent of the subtropical cloud-SST feedback highlighted in previous studies. While both mechanisms influence the magnitude of subtropical SST response, the ITCZ also plays a crucial role in determining how effectively SO-induced SST anomalies extend into the equatorial eastern Pacific. Current GCMs often simulate the remote SST response to observed SO cooling as confined south of the equator (18). Our results indicate that this limited equatorial extension may be a bias due to the model's mean-state "double-ITCZ" bias.

Constraining the tropical response to Antarctic meltwater input

Idealized CESM1 simulations and ETIN-MIP experiments both suggest that the SO-tropical Pacific teleconnections may be underestimated in current GCMs, reinforcing the possibility that the observed tropical eastern Pacific cooling trends may arise partly from the SO. While it remains unclear what causes the observed SO cooling trends and GCM warm biases, one increasingly recognized mechanism is Antarctic ice-sheet meltwater input—a process lacking in current GCMs. Accounting for Antarctic meltwater input in a variety of GCMs produces SO surface cooling and freshening response resembling observations (22, 23, 39–41). This is primarily because the meltwater-induced freshening increases upper-ocean stratification, reducing the upward heat transport from the relatively warm subsurface (39, 41). A recent study (19) found that the meltwater-induced SO cooling trends can further expand into the tropics, driving a tropical SST trend pattern closer to observations.

Here we leverage a recent community effort—the Southern Ocean Freshwater Input from Antarctica initiative (SOFIA) (42)—to examine the inter-model uncertainty in the tropical SST response to Antarctic meltwater forcing. SOFIA provides near-equilibrium meltwater hosing simulations with a constant freshwater release around Antarctica (Methods). Preliminary results from eight fully-coupled GCMs show that the addition of freshwater yields a robust SO surface cooling response and Antarctic sea-ice expansion (42, 43). We

focus on the remote tropical impact and find that the multi-model mean near-surface air temperature (TS) response (as the SST output is not readily available for all models) shows a La Niña-like tropical cooling pattern (Fig. 4C), consistent with the previous single model study (19). The magnitude of the tropical response, however, varies greatly across individual models (Fig. S6), along with a large spread in their precipitation mean state (Fig. 4A and Fig. S5). To quantify the spread in tropical TS response related to the mean-state ITCZ, we repeat the regression analysis with pr^* . As the SO TS cooling response to meltwater input is highly model-dependent, which we expect is not directly driven by tropical processes, we normalize the tropical TS response for each model by its SO TS change before performing the regression analysis.

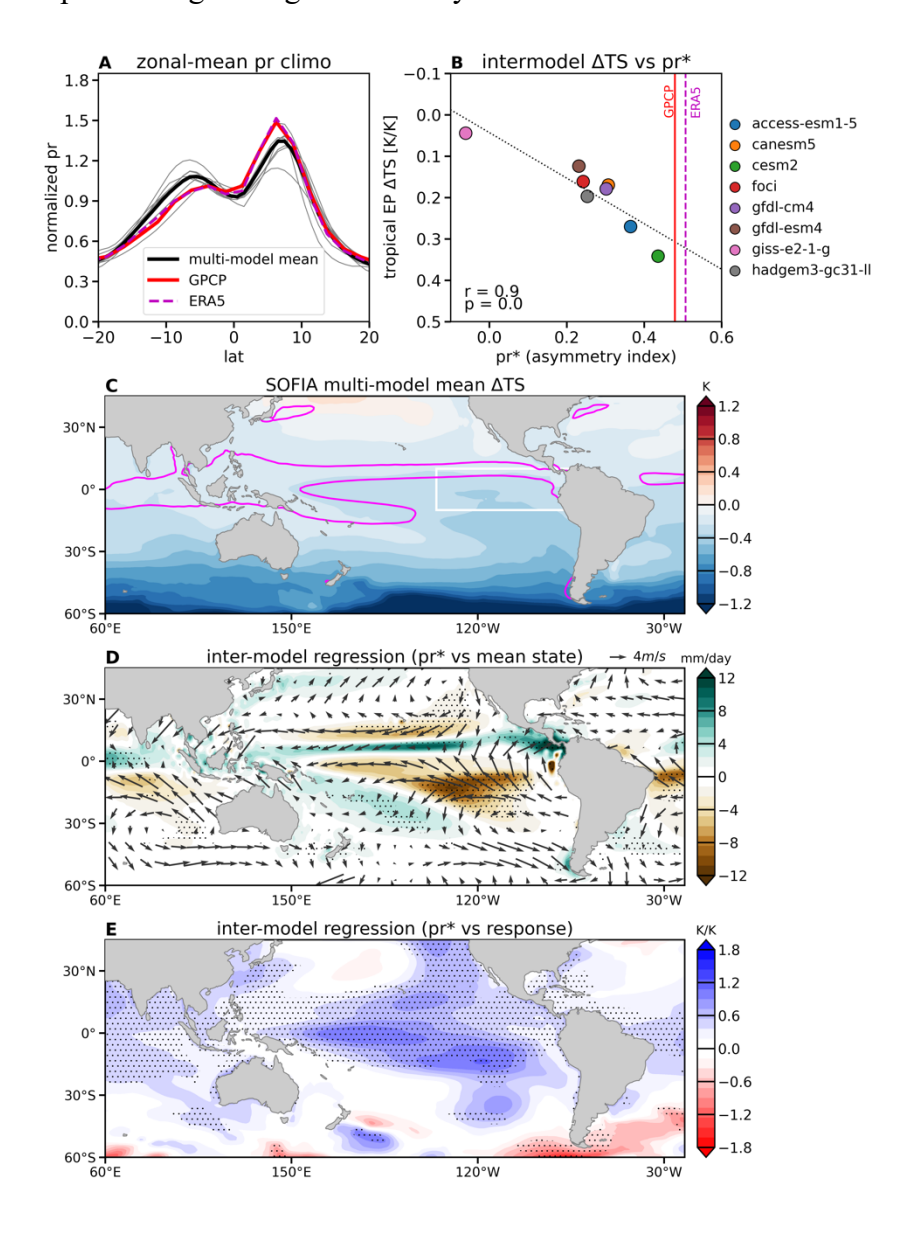


Figure 4: Mean-state climate and response to Antarctic meltwater in SOFIA meltwater experiments. (A) Annual-mean zonal-mean precipitation normalized by the tropical mean from observations and SOFIA models. Similar to Fig. 3A, except thick black line denotes the average of seven SOFIA models, and the thin grey lines denote individual models. (B) Inter-model correlation between tropical eastern Pacific TS response and mean-state pr^* . The TS response has been normalized by each model's SO (south of 60°S) TS response. (C) Multi-model mean TS and surface wind response to Antarctic meltwater input. Magenta contour denotes the 6 mm/day level of the annual-mean climatological precipitation. (D) Inter-model regression between mean-state precipitation and surface winds onto pr^* . (E) Inter-model regression between normalized TS and surface wind response onto pr^* . Stippling denotes where the inter-model regression of normalized TS is statistically significant at the 95% confidence level.

The results show that mean-state pr^* inter-model differences again explain a major portion (~80%) of the inter-model spread in the normalized tropical TS response (Fig. 4B). Intermodel regression of the tropical mean-state climate onto pr^* supports the same mechanism as in the idealized CESM1 simulations and ETIN-MIP models: models with a greater mean-state pr^* have a reduced precipitation bias in the SH tropics and therefore stronger mean-state trade winds and cross-equatorial meridional winds in the tropical eastern Pacific (Fig. 4D). These intensified mean-state winds in turn drive a stronger tropical TS response to meltwater-driven SO cooling (Fig. 4B and 4E). We note that the mean-state precipitation regression maps among the ETIN-MIP and SOFIA models, although largely resembling each other, also show slight spatial differences (Fig. 3E and Fig. 4D). For example, the ETIN-MIP models highlight wetting in the NH equatorial Pacific and Atlantic, whereas the SOFIA models highlight drying in the SH subtropical eastern Pacific and eastern Atlantic. These minor differences may arise from the different sets of models considered and the lengths of their control simulations.

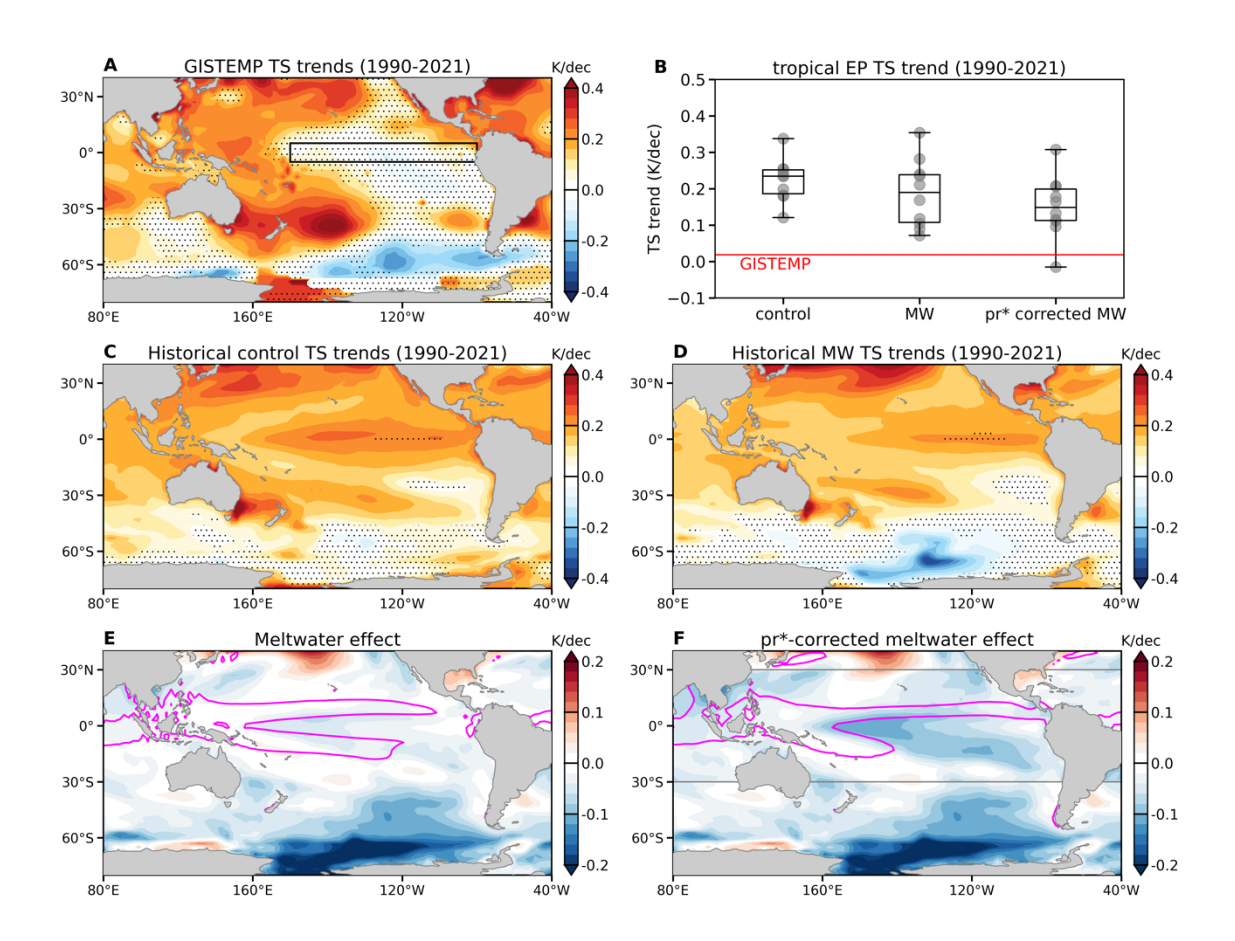


Figure 5: Observed and GISS-E2-1-G simulated TS trends over 1990–2021. (A) TS trends from the GISTEMP v4 observational dataset. (B) Tropical eastern Pacific TS trends (box in panel a) in the historical control ensemble, historical meltwater ensemble, and adjusted values based on the pr* regression and observed pr* (Methods). Note that the results of the control ensemble (left column) and the adjusted ensemble (right column) are statistically different from each other at the 95% confidence level. The box area is chosen to capture the pronounced tropical Pacific cooling over this period. (C, D) TS trends from the ensemble-mean of GISS-E2-1-G historical control and meltwater simulations. Stippling in (A, C, D) represents trend values that are not significant at the 95% confidence level. (E) TS trend difference between historical and meltwater simulations, representing the meltwater impact. Magenta contour denotes the 6 mm/day level of the annual-mean climatological precipitation from GISS-E2-1-G historical control simulations (1950–2021). (F) Similar to (E) except the tropical TS response (between 30°S–30°N, illustrated by grey lines) is adjusted based on the inter-model pr* regression (Fig. 3E), assuming that the model had reproduced the observed ITCZ.

354

355

356

357

358

359

360

361

362

363

364

365

366

367

368

369

370

371

372

373

374

375

376377378

379380

381

382

383

384

385 386

387

388

389

390

391 392

393

394

395

396

397

398

351 352

> As most models are unable to reproduce the observed ITCZ structure (Fig. 4A), their simulated tropical response may be systematically underestimated, implying that the contribution of historical Antarctic meltwater to observed tropical SST trends may have been larger. We consider an example of historical transient meltwater simulations within a CMIP6-class fully-coupled GCM, GISS-E2-1-G, where an observational estimate of Antarctic meltwater input was imposed from 1990–2021 (23, 44). Note that observational estimates of Antarctic ice imbalance based on satellite altimetry are not currently available before 1990. It has been found that the addition of meltwater flux gives rise to SO SST cooling trends (Fig. 5D), improving the model's agreement with observations (44). Beyond the SO, the meltwater input in this model produces only a marginal influence on the tropics (Fig. 5E), making insignificant differences in the simulated tropical eastern Pacific TS trends (Fig. 5B). This result seems to suggest a negligible contribution of Antarctic meltwater to the observed tropical warming pattern. However, GISS-E2-1-G appears to have a severe double-ITCZ bias (Fig. 4B and Fig. 5E), implying that its simulated SO teleconnection may be greatly underestimated. Indeed, adjusting its SOtropics teleconnection strength based on inter-model pr^* correlations (Methods), we find that the tropical impacts of Antarctic meltwater input could have been more pronounced if the model had reproduced the observed ITCZ mean state (Fig. 5F). Furthermore, accounting for both the meltwater-induced SO changes and the observationallyconstrained SO teleconnection strength brings the simulated tropical eastern Pacific TS trends into better agreement with observations (Fig. 5B). These results highlight the potentially underestimated role of Antarctic meltwater input in the observed tropical La Niña-like cooling trends.

Discussion

While the teleconnection from the tropics to the extratropics has long been established (45, 46), the reverse branch—from the SO-tropical to the tropical Pacific—remains an area of active research. There is a large uncertainty in the strength of SO teleconnections in current models, limiting our ability to robustly quantify their contributions to the observed tropical SST trends in recent decades. Using a hierarchy of model simulations with distinct SO thermal and freshwater forcings, we here demonstrate that the tropical mean-state climate, particularly the position and strength of the ITCZ, strongly modulates SO-tropical Pacific teleconnections. Models with a more realistic ITCZ tend to simulate stronger mean-state winds in the tropical eastern Pacific, which enable a stronger tropical SST response to SO forcing via mean-wind advection and the WES feedback. Given that GCMs commonly struggle with the "double-ITCZ" bias, our results imply that the remote tropical impacts of the SO may have been systematically underestimated, and that model deficiencies in the tropics may have biased our understanding of the broader impacts of polar climate change.

These results underscore the importance of improving the model mean state for accurately simulating historical climate change. For example, when forced with observed SO SST anomalies, CESM1 and CESM2 produce markedly different tropical SST responses (18, 28). The stronger tropical response in CESM2 has been attributed to its more realistic

subtropical cloud feedback (18). However, CESM2 also has a reduced double ITCZ bias compared to CESM1 (Fig. S7), which may contribute to its improvement in tropical SST trends. Thus, improving *both* cloud feedbacks and the ITCZ mean state is essential for understanding large-scale teleconnections and developing the next generation of climate models.

More broadly, improving model representation of SO teleconnections could provide new insights into tropical variability and predictability. Recent work has shown promising advances in tropical decadal prediction from improved simulations of the SO in a high-resolution GCM (47). A more realistic mean state would likely yield a stronger and more far-reaching tropical SST response to SO changes, with potential implications for equatorial variability such as ENSO.

Under increased CO_2 forcing, SO SST is projected to warm up eventually at a rate exceeding the global average (48-50). Even in recent years (post–2016), rapid sea-ice loss and ocean subsurface warming around Antarctica have occurred, indicating a possible regime shift (51, 52) in contrast to the cooling trends in earlier decades (53). The delayed future SO warming is expected to exert broad remote influences, including impacts on NH midlatitude precipitation (31) and Arctic warming (54). Advancing the representation and understanding of the SO's remote climate impacts is therefore critical for accurately constraining future global climate change.

Methods

CESM1 simulations. Simulations with mean-state modifications shown in Fig. 1 and Fig. 2 are carried out by a slab-ocean configuration of the Community Earth System Model version 1 (CESM1) with the Community Atmospheric Model version 4 (CAM4) at 2-degree horizontal resolution. All simulations are forced by a qflux climatology (e.g. prescribed ocean heat transport) and radiative forcing agents (greenhouse gases, aerosols, solar cycle, etc.) at the present-day climatological levels. The ocean mixed-layer depth is set to a uniform 50 m in all simulations to ensure consistency. We conduct three sets of simulations—"base", "cloud adjusted", and "flux adjusted"—each containing a control run and a SO-cooling experiment. For all three groups, the quasi-equilibrium responses are taken from the average of the last 30 years of the corresponding control and SO-cooling simulations.

For the "base" case, the control run is carried out for 120 years and uses a qflux climatology derived from a long piControl simulation within the fully-coupled CESM1. The corresponding SO-cooling experiment is branched from the 61st year of the control run and carried out for 60 years. Its qflux climatology is identical to that in the control run, except uniform negative qflux anomalies of 15W/m² are added over the southeast Pacific sector of the SO (55°S–35°S, 220°E–280°E), following the setup in (14).

For the "cloud adjusted" case, both the control and the SO-cooling simulations are branched from the 61st year of the "base" control simulation and carried out for another 60 years. The cloud modification is applied in both control and SO-cooling simulations, and is designed to increase the low cloud amount-SST sensitivity over the Southern Hemisphere (SH) subtropical Pacific stratocumulus deck, which is too low in CAM4 compared to the MODIS observation (36). We follow the method developed by (36), by

Science Advances Manuscript Template Page 12 of 19

adding a perturbation to all cloud layers at or below 700 hPa at every radiation time step proportional to the instantaneous SST anomaly relative to the SST mean state from the "base" control run. The cloud perturbation is set to be -3% of local low-cloud amount anomaly per degree of local SST anomaly. The modification is only applied in the CAM4 radiative transfer code to account for the radiative effect of enhanced low-cloud sensitivity. The qflux climatology data used in the control and SO-cooling simulations are identical to those used in the two "base" simulations.

The "flux adjusted" control and SO-cooling simulations are similar to the "base" simulations, except the control qflux climatology is derived from a long "flux-corrected" piControl simulation in CESM1-CAM4, where an annual-cycle of surface heat flux anomalies is applied to nudge the model's SST mean state to observations (14). The qflux anomalies over the SO are further added to this flux-adjusted qflux climatology for its SO-cooling simulation. The control run is conducted for 120 years and the SO-cooling simulation is conducted for 60 years, branched off from the 61st year of the control run.

Observations and CMIP6 models. We use precipitation observations from the Global Precipitation Climatology Project (GPCP) (55) and ERA5 Reanalysis (56). We also analyze 24 CMIP6 models and obtain the modeled precipitation climatology from their historical (1979–2014) and SSP3-7.0 (2015–2024) simulations, with one ensemble member per model. Both observed and modeled precipitation mean states are computed using annual means over 1979–2024. In Fig. 5, we use TS observations from GISTEMP v4 dataset (57) to compute the equatorial eastern Pacific TS trend over 1990–2021.

Surface energy budget analysis. We perform a mixed-layer heat budget analysis to decompose the contributions to the tropical SST response in CESM1 SO-cooling simulations. Following previous studies (15, 16, 28), we consider the surface energy budget as:

$$\rho C_p H \frac{\partial T'}{\partial t} = SW' + LW' + LH' + SH' + res (1)$$

The left hand side represents the mixed-layer heat storage, with ρ being the density of ocean, C_p the specific heat of the ocean, H the ocean mixed-layer depth and T surface temperature (i.e. SST over the ocean). The right-hand side represents the mixed-layer heat budget terms, with SW presenting surface shortwave flux, LW surface longwave flux, LH latent heat flux, SH sensible heat flux, and res residuals (all heat fluxes are defined as positive downward). The prime symbol ' represents the anomalies between the control and the SO-cooling simulations (the response). Since our CESM1 simulations are quasiequilibrium, the left hand side (the tendency term) is close to zero. Based on the linearized bulk formula for evaporation, latent heat changes associated with Newtonian cooling can be simplified as $\alpha \overline{LH}T'$ where $\alpha \equiv \frac{L_v}{R_v T^2} \approx 0.06 \ K^{-1}$, \overline{LH} is the climatological mean LH. Eq. (1) can thus be rewritten into a diagnostic equation for the SST response:

$$T' = \frac{SW' + LW' + LH'_{wind} + LH'_{RH} + LH'_{TA} + SH' + res}{\alpha \overline{LH}}$$
(2)

where LH'_{wind} , LH'_{RH} , LH'_{TA} represent latent heat trend changes due to changes in wind speed, changes in relative humidity and changes in stability, respectively.

Page 13 of 19

Science Advances Manuscript Template

Regional metrics. The precipitation asymmetry index $(pr^*, unitless)$ is defined as the difference between the NH $(0-15^{\circ}N)$ and SH $(15^{\circ}S-0)$ zonal-mean precipitation maxima, normalized by the tropical mean precipitation $(15^{\circ}S-15^{\circ}N)$. Averaging precipitation over the Pacific (e.g., between $120^{\circ}E-330^{\circ}E$) yields similar results.

The tropical east Pacific SST response presented in Fig. 3B and Fig. 4B is computed as the average over 10°S–10°N and 220°E–290°E. Changing the area or the location of the targeted region by 5° yields similar results.

The subtropical cloud feedback over the west of South America (CF_{wSA}) is computed following (17) by regressing de-seasonalized monthly shortwave cloud radiative effect (SWCRE) onto the underlying SST anomalies in the long control simulations, averaged over 260°E–290°E and 45°S–15°S. Data for the ETIN-MIP models is obtained from (17). Data for CMIP6 models (Fig. 3C) is from model piControl simulations.

SOFIA meltwater simulation. We use two experiments provided by the SOFIA project (42), piControl and antwater (in Tier 1), which are currently available for eight GCMs. The first is identical to the CMIP6 piControl setup, with no additional ice-sheet meltwater included. The second is the idealized meltwater hosing experiment, branched from the piControl simulation. It applies a freshwater flux anomaly of 0.1 Sv at the ocean surface around Antarctica. The antwater simulations are generally carried out for > 100 years, and we use the last 30 years to obtain quasi-equilibrium response. As the "tos" (seasurface temperature) and "ts" (surface temperature) variables are not readily available for most of SOFIA models, we use "tas" (near-surface air temperature) instead for the analysis. For each model, we normalize the tropical TS response by its average over Antarctica (60°S–90°S, including both ocean and land), before conducting the inter-model regression analysis.

GISS-E2-1-G meltwater simulation and analysis. The transient historical meltwater simulations within the NASA Goddard Institute for Space Studies (GISS) version E2.1 climate model (GISS-E2-1-G) are provided by and documented in (23) and (44). The control and meltwater ensembles each consist of 10 members. The control ensemble spans 1950–2021: from 1950–2014, the simulations used the CMIP6 "historical" forcing scenario with all time-varying radiative forcing agents; extensions from 2015–2021 used observed greenhouse gases and solar forcing while keeping other compositions and land use changes at 2014 levels. The meltwater ensemble builds on the control ensemble and spans the period from 1990–2021. It includes time-varying anomalous freshwater based on the observed post–1990 "ice imbalance" from Antarctica and Greenland ice sheets constrained by satellite observations (58). Meltwater is added to the Southern Ocean (500 km wide around the Antarctic continent) uniformly from the surface to 200 m below. We obtain the meltwater-induced surface temperature response by comparing the ensemble means of control and meltwater simulations (shown in Fig. 5C and Fig. 5D).

We further correct the meltwater-induced tropical TS anomalies (between $30^{\circ}\text{S}-30^{\circ}\text{N}$) based on the model's mean-state ITCZ. Specifically, we first compute the pr^* values from GISS-E2-1-G historical control simulations and ERA5 reanalysis over 1950-2021, denoted as pr_{ERA5}^* and pr_{GISS}^* , respectively. We then compute the adjusted tropical TS response ($\Delta TS_{tropics}^*$) as:

527
$$\Delta TS_{tropics}^{*}(x,y) = \left(pr_{ERA5}^{*} - pr_{GISS}^{*}\right) \frac{\partial \left(\frac{\Delta TS_{tropics}(x,y)}{\Delta TS_{SO}}\right)}{\partial pr^{*}} \Delta TS_{SO} + \Delta TS_{tropics}(x,y) (3)$$

529

530

531

532

533

534

535

536

where $\frac{\partial \left(\frac{\Delta TS_{tropics}(x,y)}{\Delta TS_{SO}}\right)}{\partial pr^*}$ represents the coefficient from the inter-model regression of normalized TS response onto pr^* across eight SOFIA models (shown in Fig. 4E), ΔTS_{SO} is the TS response averaged over the SO (60°S–90°S), and $\Delta TS_{tropics}(x,y)$ is the originally simulated tropical TS response pattern. In our estimate, we retain ΔTS_{SO} from the meltwater simulations unchanged, and only apply the pr^* adjustment to the tropical TS response pattern. The adjusted tropical response $\Delta TS_{tropics}^*(x,y)$ thus represents the more realistic tropical response to the simulated meltwater-driven SO TS changes, assuming the model had accurately reproduced the observed ITCZ (pr^*).

537538

539

Statistical Analysis

Statistical significance is evaluated using a two-sided t-test above 95% confidence level.

Regression analysis is performed using the least-square linear regression.

542543

544545

546

547 548

References

- 1. R. C. Wills, Y. Dong, C. Proistosecu, K. C. Armour, D. S. Battisti, Systematic climate model biases in the large-scale patterns of recent sea-surface temperature and sea-level pressure change. *Geophys. Res. Lett.* **49**, e2022GL100011 (2022).
- 2. M. Watanabe, S. M. Kang, M. Collins, Y.-T. Hwang, S. McGregor, M. F. Stuecker, Possible shift in controls of the tropical Pacific surface warming pattern. *Nature* **630**, 315–324 (2024).
- Y. Dong, K. C. Armour, C. Proistosescu, T. Andrews, D. S. Battisti, P. M. Forster, D. Paynter, C. J. Smith, H.
 Shiogama, Biased estimates of equilibrium climate sensitivity and transient climate response derived from historical CMIP6 simulations. *Geophys. Res. Lett.* 48, e2021GL095778 (2021).
- 552 4. M. J. Alessi, M. A. Rugenstein, Surface temperature pattern scenarios suggest higher warming rates than current projections. *Geophys. Res. Lett.* **50**, e2023GL105795 (2023).
- 554 5. M. Zhao, T. Knutson, Crucial role of sea surface temperature warming patterns in near-term high-impact weather and climate projection. *Npj Clim. Atmospheric Sci.* 7, 130 (2024).
- K. C. Armour, C. Proistosescu, Y. Dong, L. C. Hahn, E. Blanchard-Wrigglesworth, A. G. Pauling, R. C. Jnglin
 Wills, T. Andrews, M. F. Stuecker, S. Po-Chedley, others, Sea-surface temperature pattern effects have slowed
 global warming and biased warming-based constraints on climate sensitivity. *Proc. Natl. Acad. Sci.* 121,
 e2312093121 (2024).
- I. R. Simpson, T. A. Shaw, P. Ceppi, A. C. Clement, E. Fischer, K. M. Grise, A. G. Pendergrass, J. A. Screen, R.
 C. Wills, T. Woollings, others, Confronting Earth System Model trends with observations. *Sci. Adv.* 11, eadt8035 (2025).
- S. Lee, M. L'Heureux, A. T. Wittenberg, R. Seager, P. A. O'Gorman, N. C. Johnson, On the future zonal contrasts of equatorial Pacific climate: Perspectives from observations, simulations, and theories. *Npj Clim. Atmospheric Sci.* 5, 82 (2022).
- 9. R. Seager, M. Cane, N. Henderson, D.-E. Lee, R. Abernathey, H. Zhang, Strengthening tropical Pacific zonal sea surface temperature gradient consistent with rising greenhouse gases. *Nat. Clim. Change* **9**, 517–522 (2019).

Science Advances Manuscript Template Page 15 of 19

- 568 10. U. K. Heede, A. V. Fedorov, Eastern equatorial Pacific warming delayed by aerosols and thermostat response to CO2 increase. *Nat. Clim. Change* **11**, 696–703 (2021).
- 570 11. Y.-T. Hwang, S.-P. Xie, P.-J. Chen, H.-Y. Tseng, C. Deser, Contribution of anthropogenic aerosols to persistent 571 La Niña-like conditions in the early 21st century. *Proc. Natl. Acad. Sci.* **121**, e2315124121 (2024).
- 572 12. M. Watanabe, J.-L. Dufresne, Y. Kosaka, T. Mauritsen, H. Tatebe, Enhanced warming constrained by past trends in equatorial Pacific sea surface temperature gradient. *Nat. Clim. Change* 11, 33–37 (2021).
- 574 13. M. Rugenstein, S. Dhame, D. Olonscheck, R. J. Wills, M. Watanabe, R. Seager, Connecting the SST Pattern 575 Problem and the Hot Model Problem. *Geophys. Res. Lett.* **50**, e2023GL105488 (2023).
- 576 14. Y. Dong, K. C. Armour, D. S. Battisti, E. Blanchard-Wrigglesworth, Two-way teleconnections between the Southern Ocean and the tropical Pacific via a dynamic feedback. *J. Clim.* **35**, 6267–6282 (2022).
- 578 15. Y.-T. Hwang, S.-P. Xie, C. Deser, S. M. Kang, Connecting tropical climate change with Southern Ocean heat uptake. *Geophys. Res. Lett.* **44**, 9449–9457 (2017).
- 580 16. S. M. Kang, S.-P. Xie, Y. Shin, H. Kim, Y.-T. Hwang, M. F. Stuecker, B. Xiang, M. Hawcroft, Walker circulation response to extratropical radiative forcing. *Sci. Adv.* **6**, eabd3021 (2020).
- 582 17. H. Kim, S. M. Kang, J. E. Kay, S.-P. Xie, Subtropical clouds key to Southern Ocean teleconnections to the tropical Pacific. *Proc. Natl. Acad. Sci.* **119**, e2200514119 (2022).
- 18. S. M. Kang, Y. Yu, C. Deser, X. Zhang, I.-S. Kang, S.-S. Lee, K. B. Rodgers, P. Ceppi, Global impacts of recent Southern Ocean cooling. *Proc. Natl. Acad. Sci.* **120**, e2300881120 (2023).
- 586 19. Y. Dong, A. G. Pauling, S. Sadai, K. C. Armour, Antarctic ice-sheet meltwater reduces transient warming and climate sensitivity through the sea-surface temperature pattern effect. *Geophys. Res. Lett.* **49**, e2022GL101249 (2022).
- 589 20. D. L. Hartmann, The Antarctic ozone hole and the pattern effect on climate sensitivity. *Proc. Natl. Acad. Sci.* 119, e2207889119 (2022).
- 591 21. Y. Dong, L. M. Polvani, Y.-T. Hwang, M. R. England, Stratospheric ozone depletion has contributed to the recent tropical La Niña-like cooling pattern. *Npj Clim. Atmospheric Sci.* **8**, 150 (2025).
- 593 22. B. Bronselaer, M. Winton, S. M. Griffies, W. J. Hurlin, K. B. Rodgers, O. V. Sergienko, R. J. Stouffer, J. L. Russell, Change in future climate due to Antarctic meltwater. *Nature* **564**, 53–58 (2018).
- 595 23. G. A. Schmidt, A. Romanou, L. Roach, K. Mankoff, Q. Li, C. D. Rye, M. Kelley, J. C. Marshall, J. J. M. Busecke, Anomalous meltwater from ice sheets and ice shelves is a historical forcing. *Geophys. Res. Lett.* **50**, e2023GL106530 (2023).
- 598 24. M. Sigmond, M. Reader, J. Fyfe, N. Gillett, Drivers of past and future Southern Ocean change: Stratospheric ozone versus greenhouse gas impacts. *Geophys. Res. Lett.* **38** (2011).
- 25. D. Ferreira, J. Marshall, C. M. Bitz, S. Solomon, A. Plumb, Antarctic Ocean and sea ice response to ozone depletion: A two-time-scale problem. *J. Clim.* **28**, 1206–1226 (2015).
- 602 26. S. M. Kang, P. Ceppi, Y. Yu, I.-S. Kang, Recent global climate feedback controlled by Southern Ocean cooling. 603 *Nat. Geosci.* **16**, 775–780 (2023).
- S. M. Kang, M. Hawcroft, B. Xiang, Y.-T. Hwang, G. Cazes, F. Codron, T. Crueger, C. Deser, Ø. Hodnebrog,
 H. Kim, others, Extratropical-tropical interaction model intercomparison project (ETIN-MIP): Protocol and initial results. *Bull. Am. Meteorol. Soc.* 100, 2589–2606 (2019).
- 28. X. Zhang, C. Deser, L. Sun, Is there a tropical response to recent observed Southern Ocean cooling? *Geophys. Res. Lett.* **48**, e2020GL091235 (2021).

Science Advances Manuscript Template Page 16 of 19

- 609 29. Y. Zheng, M. Rugenstein, M. J. Alessi, The relationship between the Southern Ocean and the southeastern 610 subtropical Pacific in unforced and forced climate model simulations. J. Clim. (2025).
- 611 30. R. Seager, M. Hoerling, Atmosphere and ocean origins of North American droughts. J. Clim. 27, 4581–4606 612 (2014).
- 613 31. H. Kim, S. M. Kang, A. G. Pendergrass, F. Lehner, Y. Shin, P. Ceppi, S.-W. Yeh, S.-Y. Song, Higher
 - precipitation in East Asia and western United States expected with future Southern Ocean warming. Nat.
- 615 Geosci., 1–9 (2025).

- 616 32. Y. Kosaka, S.-P. Xie, Recent global-warming hiatus tied to equatorial Pacific surface cooling. *Nature* 501, 403– 407 (2013). 617
- 33. O. Adam, T. Bischoff, T. Schneider, Seasonal and interannual variations of the energy flux equator and ITCZ. 618 619 Part I: Zonally averaged ITCZ position. J. Clim. 29, 3219–3230 (2016).
- 34. B. Tian, X. Dong, The double-ITCZ bias in CMIP3, CMIP5, and CMIP6 models based on annual mean 620 621 precipitation. Geophys. Res. Lett. 47, e2020GL087232 (2020).
- 622 35. J.-Y. Zhuo, C.-Y. Lee, A. Sobel, R. Seager, S. J. Camargo, Y.-H. Lin, B. Fosu, K. A. Reed, A More La Niña-623 Like Response to Radiative Forcing after Flux Adjustment in CESM2. J. Clim. 38, 1037–1050 (2025).
- 624 36. P. Breul, P. Ceppi, P. Nowack, The importance of stratocumulus clouds for projected warming patterns and circulation changes. EGUsphere 2025, 1-22 (2025). 625
- 37. W.-T. Hsiao, Y.-T. Hwang, Y.-J. Chen, S. M. Kang, The role of clouds in shaping tropical Pacific response 626 pattern to extratropical thermal forcing. Geophys. Res. Lett. 49, e2022GL098023 (2022). 627
- 628 38. O. Adam, T. Schneider, F. Brient, Regional and seasonal variations of the double-ITCZ bias in CMIP5 models. 629 Clim. Dyn. 51, 101–117 (2018).
- 630 39. A. G. Pauling, C. M. Bitz, I. J. Smith, P. J. Langhorne, The response of the Southern Ocean and Antarctic sea ice 631 to freshwater from ice shelves in an Earth system model. J. Clim. 29, 1655–1672 (2016).
- 40. A. Purich, M. H. England, W. Cai, A. Sullivan, P. J. Durack, Impacts of broad-scale surface freshening of the 632 633 Southern Ocean in a coupled climate model. J. Clim. 31, 2613–2632 (2018).
- 634 41. C. D. Rye, J. Marshall, M. Kelley, G. Russell, L. S. Nazarenko, Y. Kostov, G. A. Schmidt, J. Hansen, Antarctic 635 glacial melt as a driver of recent Southern Ocean climate trends. Geophys. Res. Lett. 47, e2019GL086892 636 (2020).
- 637 42. N. Swart, T. Martin, R. Beadling, J.-J. Chen, M. H. England, R. Farneti, S. M. Griffies, T. Hatterman, F. A. Haumann, Q. Li, others, The Southern Ocean Freshwater release model experiments Initiative (SOFIA): 638
- 639 Scientific objectives and experimental design. EGUsphere 2023, 1–30 (2023).
- 640 43. X. Xu, T. Martin, R. L. Beadling, J. Liu, S. Bischof, T. Hattermann, W. Huo, Q. Li, J. C. Marshall, M. Muilwijk, 641 others, Robustness and mechanisms of the atmospheric response over the Southern Ocean to idealized
- 642 freshwater input around Antarctica. Geophys. Res. Lett. 52, e2024GL113734 (2025).
- 643 44. L. A. Roach, K. D. Mankoff, A. Romanou, E. Blanchard-Wrigglesworth, T. W. Haine, G. A. Schmidt, Winds and meltwater together lead to Southern Ocean surface cooling and sea ice expansion. Geophys. Res. Lett. 50, 644 645 e2023GL105948 (2023).
- 45. R. Garreaud, D. S. Battisti, Interannual (ENSO) and interdecadal (ENSO-like) variability in the Southern 646 Hemisphere tropospheric circulation. J. Clim. 12, 2113–2123 (1999). 647
- 648 46. M. A. Alexander, I. Bladé, M. Newman, J. R. Lanzante, N.-C. Lau, J. D. Scott, The atmospheric bridge: The 649 influence of ENSO teleconnections on air-sea interaction over the global oceans. J. Clim. 15, 2205-2231 (2002).

Page 17 of 19 Science Advances Manuscript Template

- 47. S. G. Yeager, P. Chang, G. Danabasoglu, N. Rosenbloom, Q. Zhang, F. S. Castruccio, A. Gopal, M. Cameron
 Rencurrel, I. R. Simpson, Reduced Southern Ocean warming enhances global skill and signal-to-noise in an
 eddy-resolving decadal prediction system. *Npj Clim. Atmospheric Sci.* 6, 107 (2023).
- 48. C. Li, J.-S. von Storch, J. Marotzke, Deep-ocean heat uptake and equilibrium climate response. *Clim. Dyn.* **40**, 1071–1086 (2013).
- 49. K. C. Armour, J. Marshall, J. R. Scott, A. Donohoe, E. R. Newsom, Southern Ocean warming delayed by circumpolar upwelling and equatorward transport. *Nat. Geosci.* **9**, 549–554 (2016).
- 50. W. Cai, L. Gao, Y. Luo, X. Li, X. Zheng, X. Zhang, X. Cheng, F. Jia, A. Purich, A. Santoso, others, Southern Ocean warming and its climatic impacts. *Sci. Bull.* **68**, 946–960 (2023).
- 51. C. Eayrs, X. Li, M. N. Raphael, D. M. Holland, Rapid decline in Antarctic sea ice in recent years hints at future change. *Nat. Geosci.* **14**, 460–464 (2021).
- 52. A. Purich, E. W. Doddridge, Record low Antarctic sea ice coverage indicates a new sea ice state. *Commun. Earth Environ.* **4**, 314 (2023).
- 53. T. Fan, C. Deser, D. P. Schneider, Recent Antarctic sea ice trends in the context of Southern Ocean surface climate variations since 1950. *Geophys. Res. Lett.* **41**, 2419–2426 (2014).
- 54. M. England, L. Polvani, L. Sun, Robust Arctic warming caused by projected Antarctic sea ice loss. *Environ. Res. Lett.* 15, 104005 (2020).
- 55. R. F. Adler, G. J. Huffman, A. Chang, R. Ferraro, P.-P. Xie, J. Janowiak, B. Rudolf, U. Schneider, S. Curtis, D.
 Bolvin, others, The version-2 global precipitation climatology project (GPCP) monthly precipitation analysis
 (1979–present). J. Hydrometeorol. 4, 1147–1167 (2003).
- 56. H. Hersbach, B. Bell, P. Berrisford, S. Hirahara, A. Horányi, J. Muñoz-Sabater, J. Nicolas, C. Peubey, R. Radu, D. Schepers, others, The ERA5 global reanalysis. *Q. J. R. Meteorol. Soc.* **146**, 1999–2049 (2020).
- 57. N. J. Lenssen, G. A. Schmidt, J. E. Hansen, M. J. Menne, A. Persin, R. Ruedy, D. Zyss, Improvements in the GISTEMP uncertainty model. *J. Geophys. Res. Atmospheres* **124**, 6307–6326 (2019).
- 58. T. Slater, I. R. Lawrence, I. N. Otosaka, A. Shepherd, N. Gourmelen, L. Jakob, P. Tepes, L. Gilbert, P. Nienow, Earth's ice imbalance. *The Cryosphere* **15**, 233–246 (2021).

Acknowledgments

The authors would like to acknowledge high-performance computing support from the Derecho system (doi:10.5065/qx9a-pg09) provided by the NSF National Center for Atmospheric Research (NCAR), sponsored by the National Science Foundation. The authors thank Dr. Hanjun Kim for sharing CF_{wSA} data for ETIN-MIP models. L.R. was supported by the Initiative and Networking Fund of the Helmholtz Association. Y.-T. Hwang and R.-J. Hu were supported by the Ministry of Science and Technology Council (NSTC), Taiwan, under Grant NSTC112-2111-M-002-016-MY4.

Author contributions: YD designed and led the research; KL performed the ``cloudadjusted" CESM1 simulations using the code developed by PB and PC. RJH and YTH performed the CMIP6 mean-state ITCZ and cloud feedback analysis. LR contributed the GISS-E2-1-G meltwater simulations. All co-authors contributed to the final draft.

Competing interests: The authors declare no competing interests.

Science Advances Manuscript Template Page 18 of 19

677 678

679

676

680 681

682 683

684

685

686 687

688 689 690

691 692

693

Data and materials availability: 694 Output from the idealized CESM1 simulations will be available on Zenodo upon 695 publication. CMIP6 data were obtained via ESGF at https://aims2.llnl.gov/search/cmip6/. 696 ALl observational data are publicly available. GPCP precipitation, ERSSTv5 SST and 697 COBE SST data were obtained from NOAA PSL at 698 https://psl.noaa.gov/data/gridded/data.gpcp.html, 699 https://psl.noaa.gov/data/gridded/data.noaa.ersst.v5.html and 700 https://psl.noaa.gov/data/gridded/data.cobe.html. ERA5 reanalysis was obtained from the 701 Copernicus Climate Data Store at https://cds.climate.copernicus.eu/datasets/reanalysis-702 era5-single-levels-monthly-means. GISTEMPv4 SST data were obtained from NASA 703 GISS at https://data.giss.nasa.gov/gistemp/. ETIN-MIP simulation output is available at 704 https://zenodo.org/records/3362615. SOFIA meltwater simulation output is available at 705 https://sofiamip.github.io/data-access.html. GISS-E2-1-G control and meltwater 706 simulation output was obtained from the NCCS portal at 707 https://portal.nccs.nasa.gov/datashare/giss_cmip6/CMIP/NASA-GISS/GISS-E2-1-G/ 708

709



Supplementary Materials for

Tropical impacts of the Southern Ocean underestimated by mean-state biases

Yue Dong et al.

*Corresponding author. Email: ydong@atmos.ucla.edu

This PDF file includes:

Figs. S1 to S7

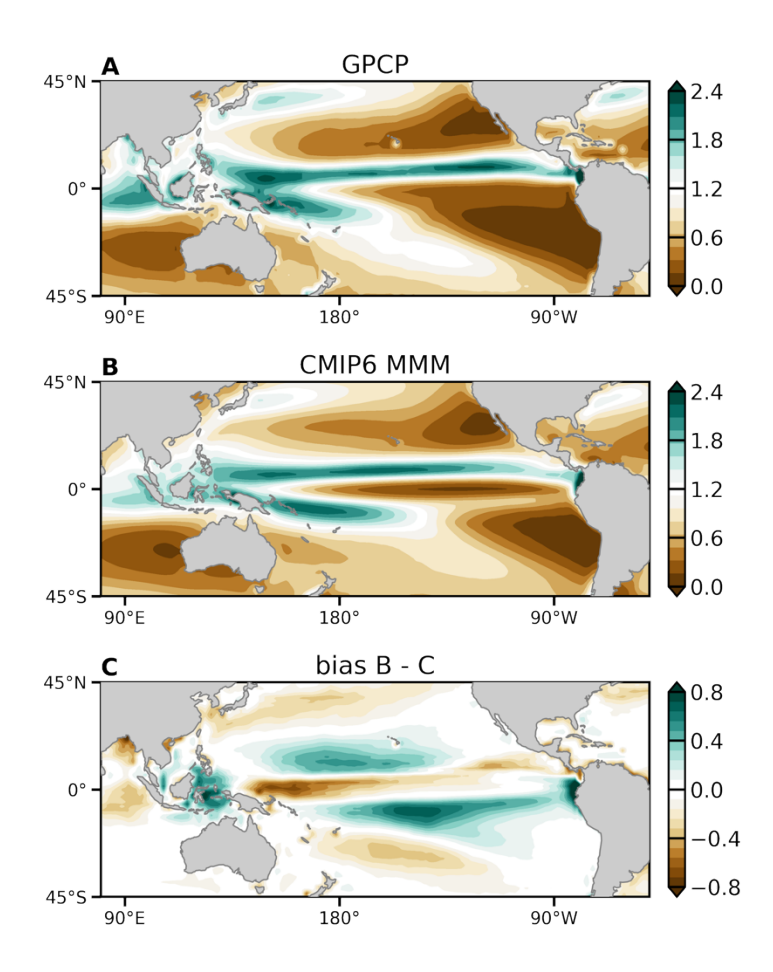


Fig. S1. Annual-mean precipitation climatology (1979-2024) in observations and CMIP6 models. (A) GPCP observations; (B) CMIP6 historical multi-model mean; (C) differences between observation and CMIP6 multi-model mean. Precipitation patterns have been normalized by the tropical mean $(15^{\circ}S - 15^{\circ}N)$.

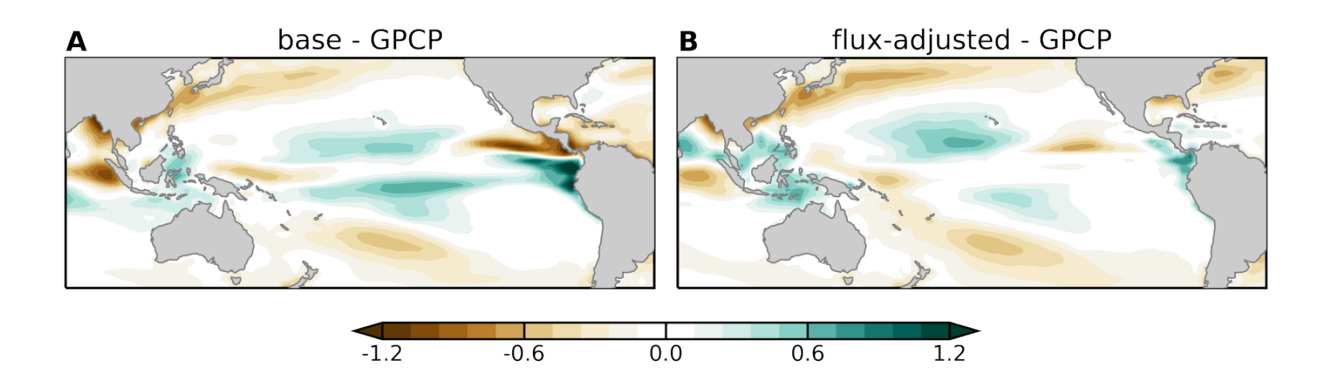


Fig. S2. Annual-mean precipitation climatology between GPCP observations and CESM1 simulations. (A) CESM1 "base" control run minus GPCP. (B) CESM1 "flux-adjusted" control run minus GPCP. Same with Figure S1, all precipitation mean states have been normalized by the tropical mean $(15^{\circ}S - 15^{\circ}N)$.

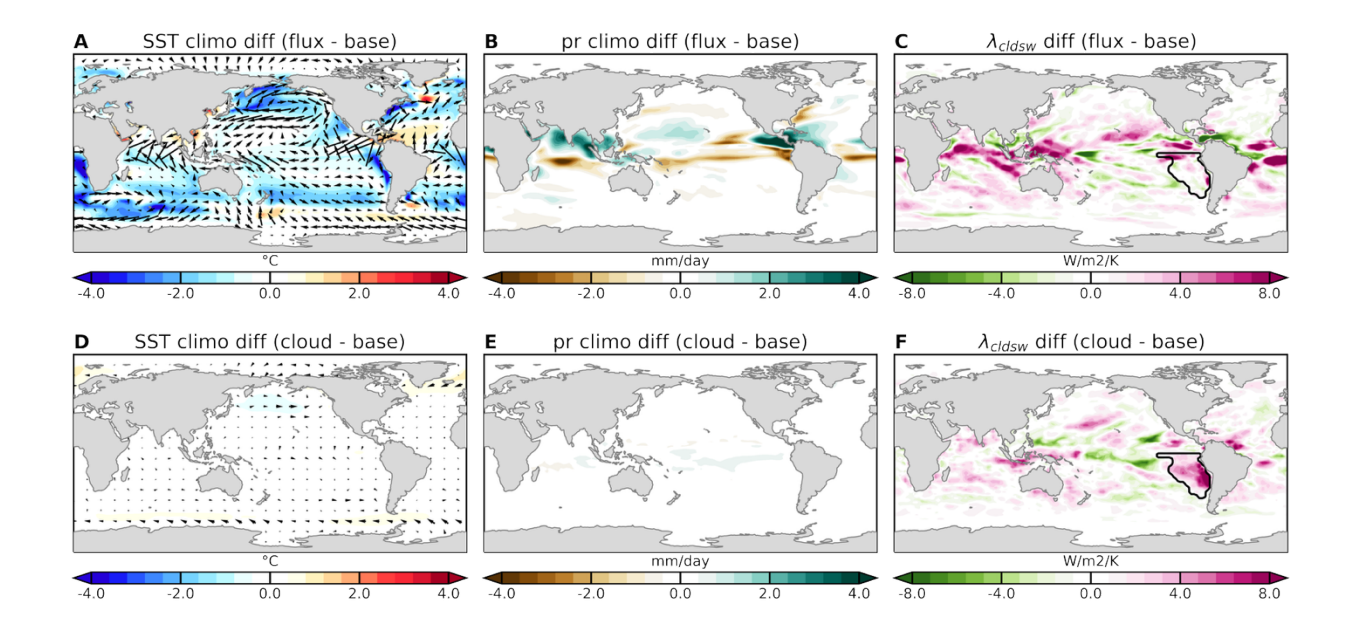


Fig. S3. Differences in mean states between "adjusted" and "base" simulations within CESM1. Top row: difference between "flux-adjusted" run and the "base" run; bottom row: difference between "cloud-adjusted" and the "base" run. From left to right are SST (K), precipitation (mm/day), and shortwave cloud feedback ($W m^{-2} K^{-1}$). Black contours in (C) and (F) illustrate the subtropical Pacific stratocumulus deck region where cloud adjustment is applied.

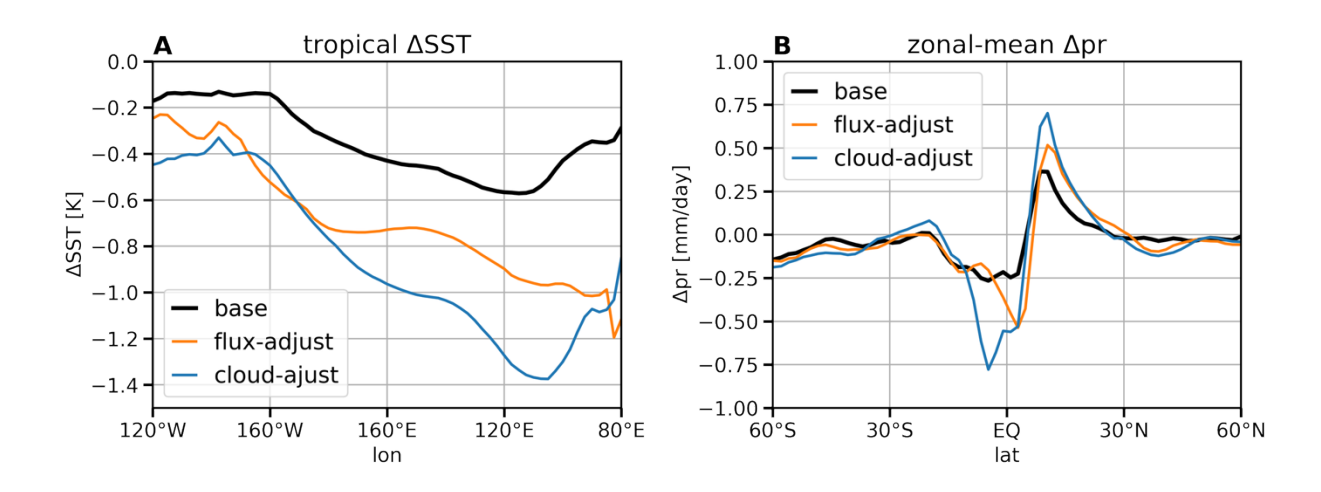


Fig. S4. Tropical SST and zonal-mean precipitation response to SO qflux forcing simulated in CESM1 simulations. (A) Tropical Pacific SST averaged over $10^oS - 10^oN$. (B) Zonal-mean precipitation between $60^oS - 60^oN$.

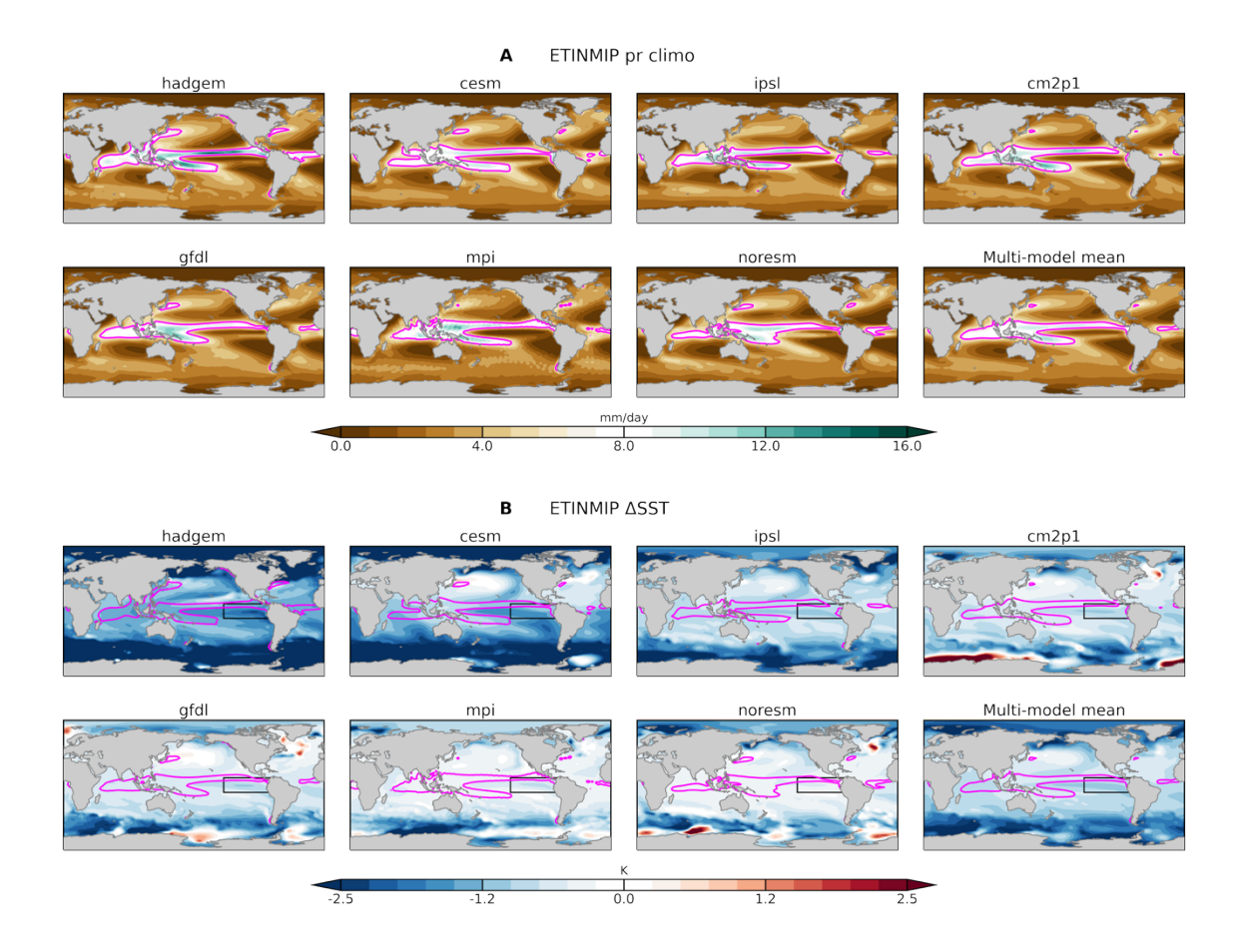


Fig. S5.
Individual ETINMIP model result. (A) mean-state precipitation from the ETINMIP control simulations; (B) SST response to imposed SH extratropical radiative forcing from the ETINMIP *stoa* simulations. Magenta contours show the 6 mm/day contour of precipitation climatology. The bottom right panels in both (A) and (B) show the multi-model mean results.

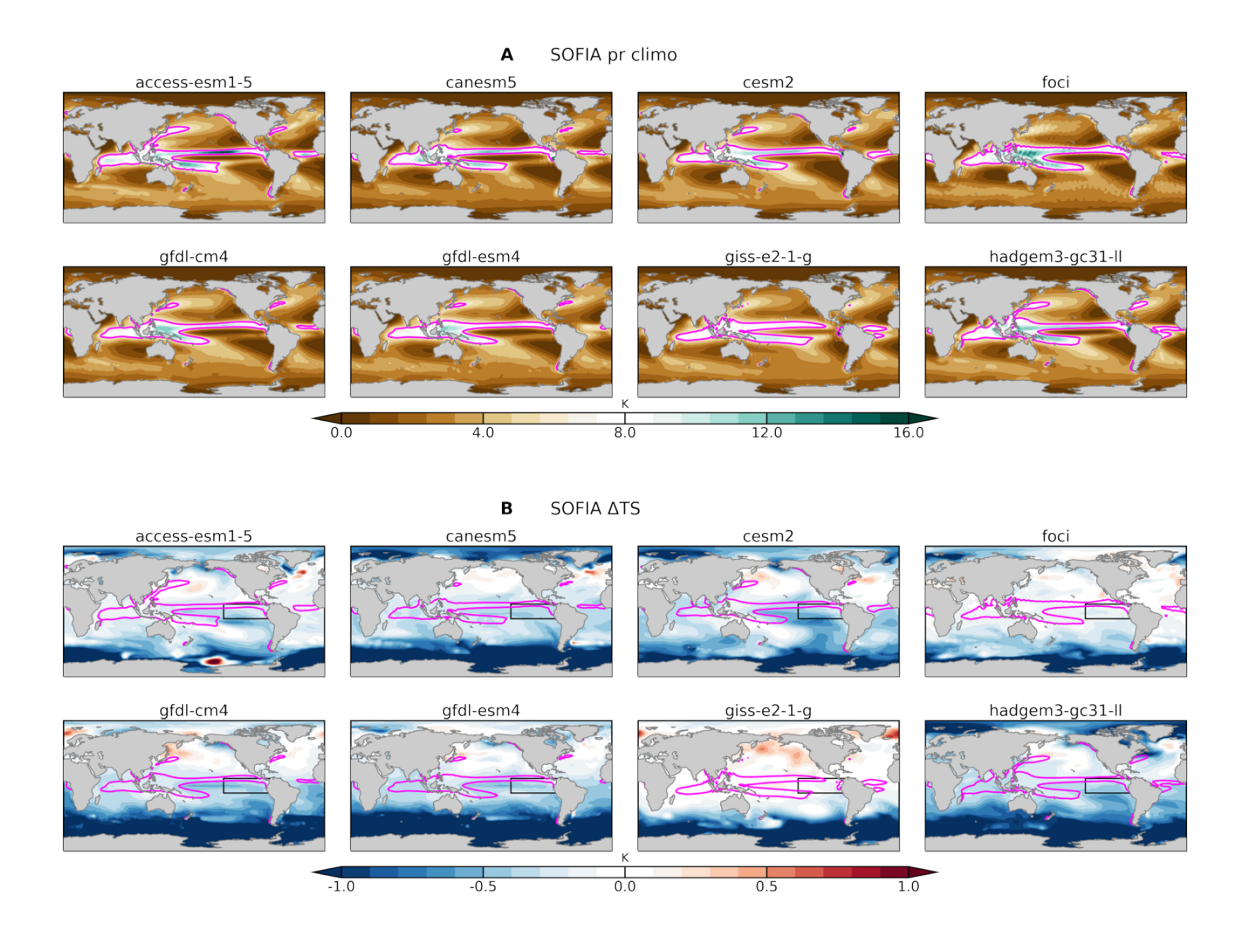


Fig. S6.Individual SOFIA model results. (A) mean-state precipitation from the SOFIA control simulations; (B) surface air temperature response to imposed Antarctic meltwater from SOFIA hosing simulations. Magenta contours show the 6 mm/day contour of precipitation climatology.

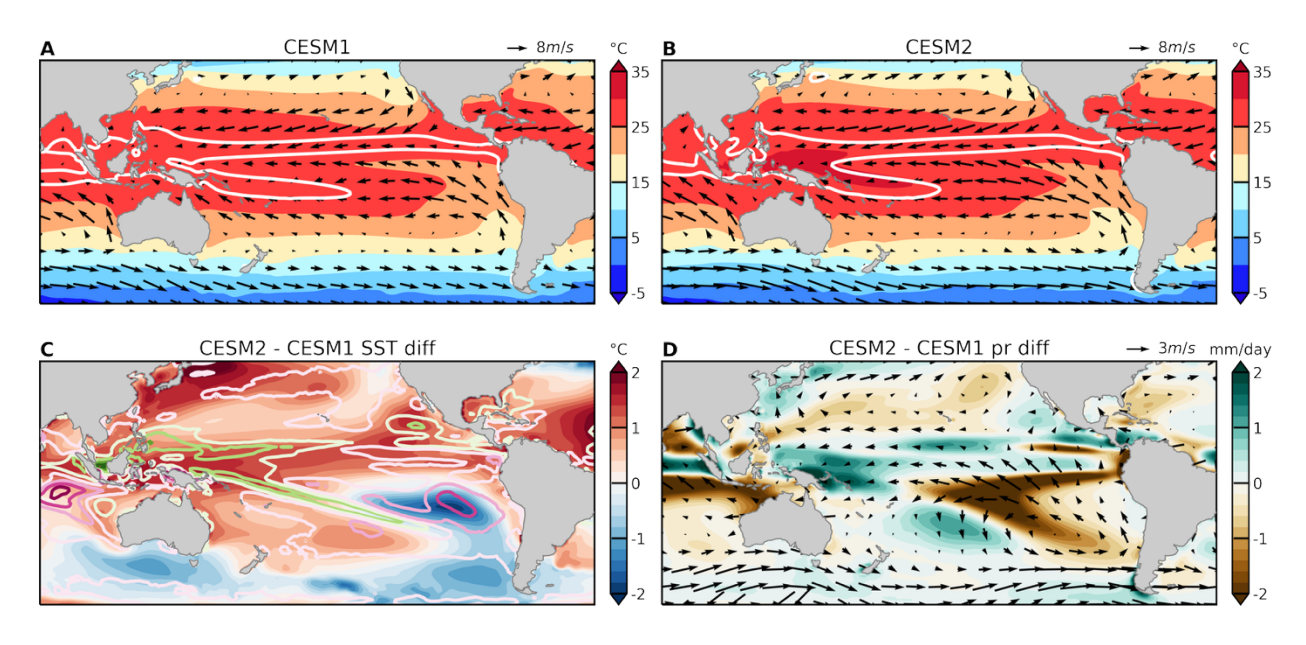


Fig. S7.

CESM1 and CESM2 mean-state climates from piControl simulations. (A-B) mean-state SST (shading), surface winds (arrows) and precipitation (6 mm/day contour) in CESM1 and CESM2. (C) Difference in SST (shading) and cloud-SST feedback (contours) between CESM1 and CESM2. Pink (green) denotes more positive (negative) cloud-SST feedback values. (D) Differences in precipitation (shading) and surface winds (arrows).